Theoretical Analysis of Heteroaromatic Thioaminyl Radicals. Part 1: A Comparison of Ab Initio and Density Functional Methods in Calculations of Molecular Geometry and Isotropic Hyperfine Coupling Constants†

Piotr Kaszynski*

Organic Materials Research Group, Department of Chemistry, Vanderbilt University, Nashville, Tennessee 37235

Received: September 23, 2000; In Final Form: June 1, 2001

Molecular parameters of 23 heterocyclic radicals containing the thioaminyl fragment were systematically investigated with ab initio and DFT methods. Several basis sets were used to establish correlations between calculated and experimental geometries and isotropic hyperfine coupling constants. Distribution of spin and charge densities in the radicals was analyzed using the UB3LYP/6-31G* method. The data were subsequently analyzed with an emphasis on the quality of correlation rather than on the absolute accuracy of the calculated values. This resulted in a set of empirical scaling factors relating the calculated and experimental hfcc for cyclic thioaminyl radicals and provided a tool for routine design, structural elucidation, and characterization of new radicals. The protocol is used in the critical analysis of hfcc for several previously reported radicals. A companion paper (ref 1) follows in this issue [Kaszynski, P. *J. Phys. Chem. A* **2001**, *105*, 7626].

Introduction

Over the past decade, heterocyclic radicals containing the thioaminyl fragment −N−S− have become attractive building blocks for molecular conductors[2−7] and magnetic materials.[8−13] Extensive studies of these neutral π radicals resulted in several dozen well-characterized structures[14−17] (e.g., **1**−**11** in Figure 1), which are typically high-melting solids but some derivatives form paramagnetic liquids.[18,19] Structural versatility of the −N−S− fragment and the generally observed relatively high chemical and thermal stability of the heterocycles provides opportunities for further investigation of new radicals and materials. In this context, we began study of these radicals as potential structural elements for a new class of liquid crystals.[20−23]

One of the critical factors necessary for further progress in the study and application of thioaminyl heterocycles is the ability to predict a priori their properties and to guide the experimental work. This, in turn, relies on the development of reliable theoretical description of the known systems and devising appropriate and convenient computational protocols for new radicals.

Calculations of molecular and electronic structures of cyclic thioaminyl radicals have been performed using semiempirical methods[6,14,20,24−30] and more recently with the Hartree−Fock (HF), MP2, and DFT methods.[2,29−37] There have been, however, no systematic and comprehensive computational studies for these radicals. The semiempirical methods yield a qualitative understanding of the electronic structures, and only the inclusion of correlation treatment such as CASSCF and MP(n) gives reasonably good agreement with the experimental data.[33,34] While the CI and Møller−Plesset methods are prohibitively expensive for large molecular systems, density functional methods (DFT) provide an attractive, low-cost alternative.

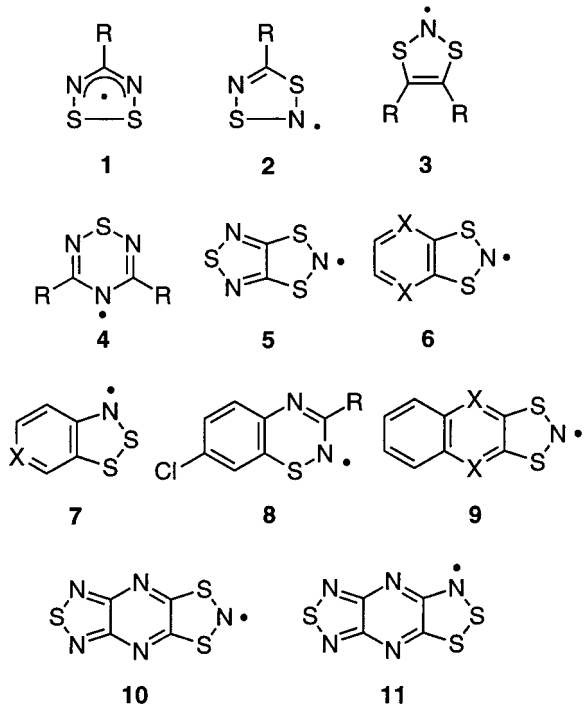

a R=H, **b**, R=F; **c**, R=Cl, **d**, R=CH_3; **e**, R=CF_3; **f**, R=CN; **g**, R=Ph **h**, X=CH; **i**, X=N

Figure 1. Selected resonance structures for radicals **1**−**11**.

Density functional theory[38] methods, and Becke-type[39] hybrid functionals in particular, have been shown to perform exceptionally well in ground state open-shell systems that are either electrically neutral[40−43] or charged.[44,45] This has been attributed to the inclusion of some electron correlation by a combination of exchange functionals with local and gradient-corrected correlation functionals. It has been found that HF−DFT

† Presented, in part, at 215th ACS National Meeting, March 29−April 2, 1998, Dallas, TX, Abstr: COMP 145; and at the Structural and Mechanistic Organic Chemistry: A Tribute to Norman L. Allinger, Athens, GA, June 3−7, 1997.

* Phone/fax: (615) 322-3458. Email: piotr@ctrvax.vanderbilt.edu.

10.1021/jp003459o CCC: $20.00
Published on Web 07/25/2001

TABLE 1: Fermi Contact (F_x) Hyperfine Coupling Constants (A_x) Conversion Factors C_X for Selected Nuclei (A_X [MHz] = $C_X \bullet F_X$)

X	^{1}H	^{13}C	^{14}N	^{15}N	^{19}F	^{33}S	^{35}Cl [a]	^{37}Cl
C_X	4469.616	1123.854	322.960	−452.999	4204.929	342.897	437.949	364.535

[a] Weighted C_{Cl} for natural isotopic ratio (75.8% of ^{35}Cl and 24.2% of ^{37}Cl) is 420.183.

methods, particularly B3LYP[46] with the 6-31G(d) basis set, accurately reproduce the experimental hyperfine coupling constants (hfcc).[43,47,48] Other molecular parameters such as spin populations,[49] ionization potential energies,[50] and IR frequencies[42] calculated with DFT methods are also in excellent agreement with the experimental values.

Here, we describe our efforts to develop a practical computational protocol for designing new thioaminyl radicals. We evaluate the performance of the UB3LYP and UHF methods, with an emphasis on the quality of their reproduction of experimentally known molecular and electronic parameters of radicals **1**−**11**. First, we establish the structures of conformational minima of compounds containing the CH_3, CF_3, and Ph groups and compare the calculated geometries with those obtained by gas-phase electron diffraction techniques. Second, the isotropic hfcc are calculated and compared with the experimental results. Third, we discuss the spin and charge distribution in the thioaminyl radicals. In the accompanying paper, we focus on redox processes involving radicals **1**−**11**.[1]

Computational Methods

General. Quantum mechanical calculations were carried out using the Gaussian 94 package[51] on an SGI R8000 workstation. Geometry optimizations were undertaken using appropriate symmetry constraints and default convergence limits. The computations employed the 6-31G(d) basis set, occasionally augmented with high angular momentum functions,[52] and Dunning's cc-pVDZ basis set.[53] The basis sets were used as supplied by the Gaussian program. DFT computations used unrestricted Becke's[46] three-parameter hybrid functional together with the nonlocal correlation functional of Lee, Yang, and Parr[54] (UB3LYP). Vibrational frequencies, calculated using the UHF/6-31G(d) and UB3LYP/6-31G(d) levels of theory, were used to characterize the nature of the stationary points and to obtain thermodynamic parameters. Zero-point energy (ZPE) corrections obtained using the UHF and the UB3LYP methods and the 6-31G(d) basis set were scaled by 0.9135 and 0.9804, respectively.[55]

Isotropic Hyperfine Coupling Constants (hfcc). The Fermi contact values F_X calculated for an atom X were converted into hfcc expressed in MHz using eq 1, in which μ_x is the atomic magnetic moment and I_x the nuclear spin number.[56] The constants in eq 1 are substituted with a new constant C_X in eq 2 characteristic for a nucleus X and values for selected nuclei are listed in Table 1.[57]

$$A_X\,[\mathrm{MHz}] = 800.237777(\mu_x/I_x)F_X \quad (1)$$

$$A_X\,[\mathrm{MHz}] = C_X F_X \quad (2)$$

$$A_X\,[\mathrm{MHz}] = 28.0247(g/g_e)a_x \quad (3)$$

Experimental hfcc values expressed in mT were converted to MHz units using eq 3 where g and a_x are the experimental values. Some of the experimental ESR results are discussed in recent reviews.[15,58]

Computational results for radicals **1**−**11** including energies, hfcc, and spin densities are listed in Supporting Information.

Results and Discussion

In almost all heterocyclic radicals studied to date, the thioaminyl fragment is a part of a longer, three- or four-membered array of heteroatoms such as −N−S−S−N− (**1a**,[35] **1b**,[28] **1c**,[28] **1d**,[59] **1e**,[28,60] **1g**[59,61]), −N−S−N−S− (**2d**[29,62]), −N−S−N− (**4c**,[27] **4e**,[27] **4g**,[24] **5**,[63] **10**[64]), −S−N−S− (**3a**,[62,65] **3e**,[30] **3f**,[66,67] **5**,[63] **6h**,[68,69] **6i**,[66] **9h**,[64] **9i**,[66] **10**[64]), and −N−S−S− (**7h**,[62,70] **7i**,[71] **11**[6]), as shown in Figure 1. Radicals containing the −S−N− fragment connected directly to the carbon framework are rare, and **8**[72] as well as two compounds recently reported by us[23] are the only examples. There have been relatively few parent radicals synthesized and studied in detail. Many of them carry substituents such as halogen, phenyl, CH_3, or CF_3 that stabilize the radicals and/or simplify their syntheses. For more accurate considerations of radical properties we first establish their ground-state geometries and conformational preferences.

Conformational Analysis. Generally, the barrier to the internal rotation of CH_3 and CF_3 groups in the heterocyclic derivatives is low, about 1.5 kcal/mol at room temperature (Figure 2). This is consistent with a gas-phase electron diffraction study for **1e**, which concluded that the CF_3 group freely rotates at 300 K.[28]

The UHF/6-31G(d) calculations disagree with the DFT results predicting conformational minima for the eclipsed forms **1d**−**A** and **1e**−**A**. The solid-state structures of **1e** and its cation **1e**$^{+}$ [28] indicate that the staggered conformation is a shallow minimum on the potential energy surface, which is consistent with the results of UB3LYP calculations.

A conformational minimum in radical **2d**, an isomer of **1d**, was found for **2d**−**A** in which the CH_3 hydrogen eclipses the nitrogen atom. The conformer **2d**−**B** in which one of the CH_3 hydrogen atoms eclipses the sulfur atom represents a transition state for the internal rotation of the methyl group. A minimum with a pseudo staggered conformation was not found.

Compound **3e** constrained at C_{2v} symmetry with the fluorine atoms eclipsing the sulfur atoms appears to represent a transition state in both the UB3LYP and UHF methods. Relaxing the C_{2v} symmetry of **3e**−**A** to C_2 in conformer **3e**−**B** alleviates some of the steric repulsion by twisting the CF_3 groups by about 17° with respect to the ring plane. This is consistent with a recent report, which concluded that the motion of the two CF_3 groups is correlated.[73]

The conformational potential energy surface of **4e** is complex due to the presence of two independent CF_3 groups, which may adopt either eclipsed or staggered orientations with respect to the ring. In contrast to the results for **1e**, the UHF and UB3LYP calculations agree that the eclipsed conformer **4e**−**A** represents the global minimum. The two other eclipsed conformers, **4e**−**B** and **4e**−**C**, are the first and the second-order transition states, respectively. The barrier to the internal rotation of the CF_3 group has been calculated to be about 1.5 kcal/mol, which is similar to the value obtained for **1e** (Figure 2). The two staggered conformations with the CF_3 groups anti (C_2 symmetry) and syn (C_s symmetry) are the hilltops on the potential energy surface.

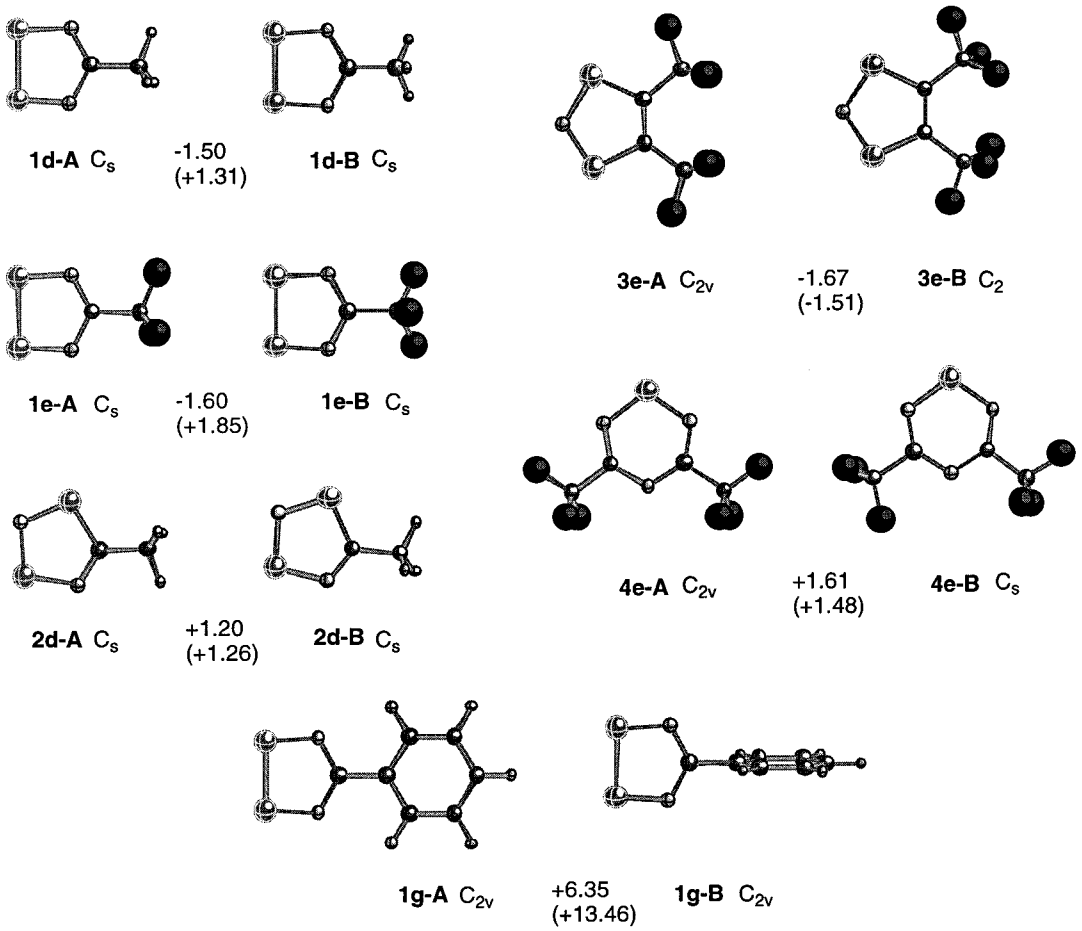

Figure 2. Ball and stick representations of conformational minima and maxima, and the free energy difference between the forms **B** and **A** calculated using UB3LYP/6-31G(d) and UHF/6-31G(d) (in parentheses) methods.

Phenyl rings in **1g** and **4g** prefer orientations coplanar with the heterocyclic rings, according to UB3LYP/631G(d) calculations. This is consistent with the UHF/6-31G(d) results for **1g** only, since no stable wavefunction could be obtained for **4g** at this level of theory. The gas-phase calculations find some support in the solid-state molecular structures of **4g**,[24] **1g**,[74] their cations,[24,75,76] and some other derivatives,[15] which all demonstrate the coplanarity of the rings. The barrier to the internal rotation of the phenyl ring in **1g** was calculated to be 6.4 kcal/mol at the UB3LYP/6-31G(d) level of theory, which is about half of that obtained with the UHF/6-31G(d) method.

Due to the large size of the calculations, the conformational preference of the phenyl group in **8g** was not investigated and the aromatic ring was constrained to coplanarity with the heterocyclic ring.

Conformers representing the global minima were used in the subsequent calculations.

Molecular Geometry. Heterocycles **1e**[28] and **3e**[18] are the only two radicals whose geometry was studied by the electron diffraction technique in the gas phase where the radicals do not form dimers. Molecular geometry optimization for these radicals was performed for their conformational minima using the UHF (**1e**−**A** and **3e**−**B**) and the UB3LYP (**1e**−**B** and **3e**−**B**) methods with several basis sets. The results are compared with the experimental data and both are shown in Tables 2 and 3.

Both the Hartree−Fock and Becke-type hybrid functional methods reproduce the experimental molecular dimensions closely, and their accuracy is basis set dependent. Statistical analysis of the differences between the calculated and experimental values for **1e** and **3e** shown in Table 4 indicates that both methods overestimate most distances; nevertheless, the UHF performs better than the UB3LYP method for comparable basis sets. The mean deviation of distances decreases from 1.0 pm for 3-21G(d) to 0.2 pm for 6-31G(2df) basis sets in the UHF method. A similar trend is observed for the B3LYP method, and the more complete basis sets give lower mean differences (1.7 pm for the 6-31G(2df) basis set). The calculations at the UB3LYP/cc-pVDZ level of theory give a relatively large error, as compared to calculations with other basis sets.

The mean difference in the calculated and experimental interatomic angles shows low basis set sensitivity. As observed for the interatomic distances, the UHF method is superior to the UB3LYP method and gives negligibly small mean errors and standard deviations (about 1°), half the value of those obtained with the UB3LYP method. Incidentally, the UB3LYP results are virtually identical to those recently reported for **3e** obtained with UB1LYP method.[73]

Based on this limited number of data points, the UHF method appears to be more accurate for geometry calculations than the more expensive UB3LYP method. The UHF/6-31G(d) method gives results close to the experiment, and they are within three times the experimental uncertainty (0.6 pm and 0.7°). However, the accurate prediction of the distances involving the sulfur atoms remains problematic in both methods and requires high angular momentum functions. For instance, the mean error for the S−S, S−N, and S−C distances is reduced from 1.2 pm (UHF/6-31G(d)) to 0.1 pm (UHF/6-31G(2df)).

A comparison of molecular dimensions shows that there is no significant difference between the two conformers **1e**−**A** and **1e**−**B**, according to calculations with the 6-31G(d) basis set.

TABLE 2: Experimental and Calculated Geometries of 1e

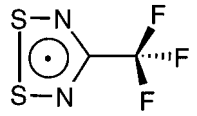

1e

	distances [ppm]					angles [deg]			
method	S−S	N−S	N−C	C−C	C−F[a]	N−C−N	S−S−N	S−N−C	F−C−F[a]
UHF/3-21G(d) [b]	212.9	165.1[a]	133.1[a]	149.0	134.3	122.3	93.6[a]	115.3[a]	108.0
UHF/6-31G(d) [b]	209.5	164.7[a]	132.3[a]	151.5	131.5	124.1	94.2[a]	113.8[a]	108.2
UHF/6-31G(2df)[b]	209.1	162.9[a]	131.9[a]	152.0	130.6	123.8	94.1[a]	113.9[a]	108.3
UB3LYP/3-21G(d)	226.6	163.8	133.7	150.1	136.7	122.9	91.5	114.2	108.3
UB3LYP/6-31G(d)	217.9	165.0	133.0	152.5	134.2	125.1	93.1	114.3	108.4
UB3LYP/6-31G(2df)	215.4	163.7	132.6	152.8	133.3	124.7	93.4	114.8	108.4
UB3LYP/cc-pVDZ	218.2	166.0	133.1	152.7	134.3	125.6	93.2	114.0	108.1
experimental[c]	211.3(6)	162.3(3)	131.8(6)	151.7(12)	133.3(4)	124.4(11)	93.9(5)	113.9(6)	107.4(5)

[a] Average values. [b] Geometry was constrained at the C_s symmetry with the N−C−C−F dihedral angle set to 0°(eclipsed conformation) and the resulting values were weight averaged. [c] Gas-phase electron diffraction studies. Höfs, H.-U.; Bats, J. W.; Gleiter, R.; Hartmann, G.; Mews, R.; Eckert-Maksić, M.; Oberhammer, H.; Sheldrick, G. M. *Chem. Ber.* **1985**, *118*, 3781.

TABLE 3: Experimental and Calculated Geometries of 3e[a]

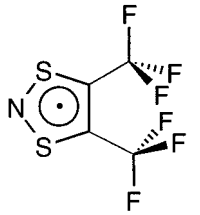

3e

	distances [pm]					angles [deg]					
method	S−N	S−C	C−C	C−CF_3	C−F[b]	S−N−S	C−S−N	C−C−S	F−C−F[b]	C−C−CF_3	F−C−C−C
UHF/3-21G(d)	167.1	175.7	131.4	149.0	134.6	116.2	96.3	115.7	107.7	126.4	160.5
UHF/6-31G(d)	166.2	176.3	132.1	151.0	131.7	115.1	97.6	114.9	107.9	127.3	160.0
UHF/6-31G(2df)	164.0	175.4	132.0	151.3	130.8	115.2	98.0	114.4	107.9	127.4	160.3
UB3LYP/3-21G(d)	170.4	175.7	133.9	149.1	137.2	113.1	98.1	115.4	108.0	126.3	161.9
UB3LYP/6-31G(d)	168.6	176.3	134.8	150.9	134.6	113.3	98.8	118.4	107.9	127.0	163.4
UB3LYP/6-31G(2df)	166.4	175.3	134.6	151.1	133.7	113.6	99.0	114.2	107.9	127.2	163.5
UB3LYP/cc-pVDZ	169.5	176.8	135.2	151.1	134.6	112.8	99.0	114.6	107.7	127.3	162.8
experimental[c]	163.4(4)	174.9(5)	132.4(14)	148.1(6)	133.0(3)	117.3(9)	96.5(12)	114.8(6)	107.4(3)	127.3(5)	*d*

[a] Geometry was constrained at the C_2 symmetry. [b] Average value. [c] Gas-phase electron diffraction studies. Awere, E. G.; Burford, N.; Mailer, C.; Passmore, J.; Schriver, M. J.; White, P. S.; Banister, A. J.; Oberhammer, H.; Sutcliffe, L. H. *J. Chem. Soc., Chem. Commun.* **1987**, 66. [d] Not reported.

TABLE 4: Statistical Analysis of the Differences between the Theoretical and Experimental Molecular Geometries of 1e and 3e[a]

	distances [pm], n=10		angles [deg], n=9	
method	mean	STD	mean	STD
UHF/3-21G(d)	1.0	1.8	−0.2	1.1
UHF/6-31G(d)	0.5	1.8	0.0	0.9
UHF/6−31(2df)	0.2	1.8	0.0	1.0
UB3LYP/3-21G(d)	3.5	4.7	−0.6	1.8
UB3LYP/6-31G(d)	2.6	1.9	0.3	2.1
UB3LYP/6−31(2df)	1.7	1.3	0.0	1.7
UB3LYP/cc-pVDZ	2.9	2.1	−0.1	1.9
experimental		0.6		0.7

[a] The number of datapoints is indicated by *n*.

The largest differences of 0.1 pm are observed for the N−S (UHF) and S−S (UB3LYP) bond lengths, and 0.1° for the N−C−N angle (UHF).

Isotropic Hyperfine Coupling Constants. Fermi constants were calculated for **1**−**11** using the UHF and UB3LYP methods and converted to hfcc using eq 2. For the purpose of comparison with the experimental data, the hfcc for the conformationally mobile CH_3 (**1d** and **2d**) and CF_3 (**1e**, **3e**, and **4e**) derivatives were calculated as average values for two conformers. The ^{1}H and ^{19}F hfcc for the CX_3 groups were calculated as average values for each conformer. The experimental hfcc were used for comparison with the calculated values according to the original structural assignment with the exception of **9i** and **11**, in which the assignment was switched to keep consistency with the computational trends. Hfcc reported as average values for two or more nuclei were used to compare individually to each calculated value. Thus the average A_N in **4g** and A_H in **6h** were compared to two calculated values each. The experimental and theoretical ^{15}N hfcc in **3e** and **6i** were scaled by C_{14N}/C_{15N} = 0.7129 (see Table 1) and compared as respective ^{14}N hfcc values. The ^{1}H hfcc assignment reported[71] for **7i** is ambiguous and was not used in the present comparison.

The results of statistical analysis of the data sets are shown in Table 5. Selected correlations between absolute theoretical and experimental ^{14}N, ^{33}S, ^{1}H, and ^{19}F hfcc are shown in Figure 3, and the best fit linear functions are listed in Table 6.

The analysis shows that the UHF method generally performs poorly, while all DFT calculations give hfcc close to the experimental values. This generally observed remarkable effectiveness of the DFT methods is due, in part, to the incorporation of some correlation effects and, in part, to minimum spin contamination. The initial small spin contamination in the UB3LYP wavefunctions is effectively annihilated,

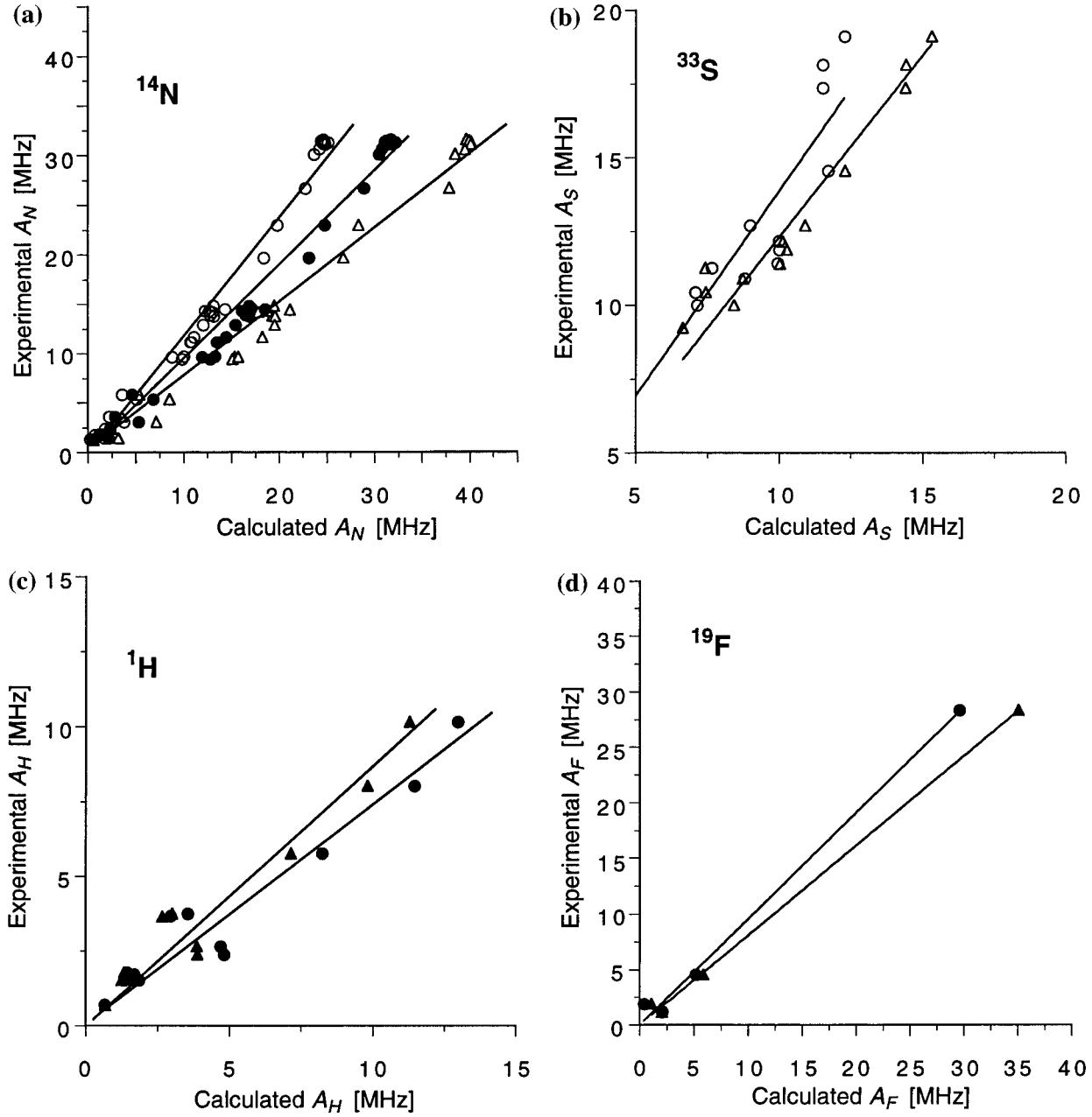

Figure 3. Selected plots of theoretical vs experimental isotropic hfcc for ^{14}N (a), ^{33}S (b), ^{1}H (c), and ^{19}F (d) nuclei in radicals **1**−**11** calculated using UB3LYP/6-31G(d) (full circles), UB3LYP/6-31G(2df)//UB3LYP/6-31G(d) (open circles), UB3LYP/cc-pVDZ//UB3LYP/6-31G(d) (full triangles), and UB3LYP/cc-pVDZ//UHF/6-31G(d) (open triangles) methods. The slopes *m* and correlation factors R^2 are listed in Table 6.

TABLE 5: Mean and Standard Deviation of the Difference between the Experimental and Calculated hfcc [MHz][a]

	^{14}N			^{33}S			^{1}H			^{19}F		
method	*n*	mean	STD	*n*	mean	STD	*n*	mean	STD	*n*	mean	STD
UHF/6-31G(d)	33	−39.8	16.0	13	−1.73	3.11	12	−25.2	33.0	4	−77.1	133.6
UB3LYP/6-31G(d)	36	−1.43	1.43	13	5.54	2.65	12	−0.99	1.50	4	−0.33	1.23
UB3LYP/6-31G(2df)// UB3LYP/6-31G(d)	35	2.38	2.64	13	3.71	1.80	12	−0.54	1.07	4	−1.80	1.67
UB3LYP/6-31G(2df)	18	2.91	2.88	9	3.15	1.92	6	−0.16	0.93	3	−1.60	1.89
UB3LYP/cc-pVDZ// UB3LYP/6-31G(d)	36	−5.20	2.83	13	2.63	1.30	12	−0.38	0.96	4	−2.05	3.27
UB3LYP/cc-pVDZ// UHF/6-31G(d)	33	−5.32	3.35	13	2.52	0.88	12	−0.36	1.16	4	−0.24	1.34

[a] The number of datapoints is indicated by *n*.

and the resulting S^2 operator values are indistinguishable from that for the pure doublet ($S^2 = 0.75$). In contrast, the initial spin contamination in the UHF method is substantial, and even after annihilation it remains high, artificially increasing spin densities especially for **1g**, **7**, **8**, and **11** ($1.0 < S^2 < 4.7$). This has an impact on the calculated hfcc values, since they are

TABLE 6: Best Fit Lines and Correlation Factors R^2 for the Theoretical and Experimental hfcc [MHz][a] ($A_{exp} = m \bullet A_{calc}$)

	^{14}N			^{33}S			^{1}H			^{19}F		
method	*n*	*m* (% error)	R^2	*n*	*m* (% error)	R^2	*n*	*m* (% error)	R^2	*n*	*m* (% error)	R^2
UHF/6-31G(d)	33	0.30 (6.7)	0.608	13	0.861 (6.0)	0.233	12	0.09 (21)	0.12	4	0.09 (6.4)	0.980
UB3LYP/6-31G(d)	36	0.937 (1.4)	0.978	13	1.73 (5.5)	0.350	12	0.744 (5.1)	0.923	4	0.953 (3.5)	0.994
UB3LYP/6-31G(2df)// UB3LYP/6-31G(d)	35	1.202 (1.4)	0.980	13	1.388 (3.7)	0.696	12	0.834 (4.8)	0.932	4	0.865 (2.1)	0.998
UB3LYP/6-31G(2df)	18	1.232 (1.7)	0.983	9	1.324 (4.3)	0.763	6	0.866 (9.5)	0.800	3	0.882 (0.7)	0.999
UB3LYP/cc-pVDZ// UB3LYP/6-31G(d)	36	0.767 (1.2)	0.983	13	1.252 (2.5)	0.867	12	0.865 (4.6)	0.938	4	0.806 (2.3)	0.998
UB3LYP/cc-pVDZ// UHF/6-31G(d)	33	0.760 (1.2)	0.986	13	1.231 (1.9)	0.920	12	0.844 (5.5)	0.915	4	0.992 (3.9)	0.993

[a] The number of datapoints is indicated by *n*.

directly proportional to the spin densities on the s orbital which, in turn, depends on the total spin density on the entire atom.[77]

Statistical analyses shown in Table 5 indicate that the ^{14}N, ^{1}H, ^{19}F hfcc calculated with DFT are generally larger, while the ^{33}S hfcc are smaller than the experimental values. The difference between the experimental and calculated values is significantly basis set dependent, which results from differences in balancing orbital spin polarization effects in different basis sets.[45] For instance, results obtained for **1a** show that the ^{14}N isotropic hfcc ranges from $A_N = 16.15$ MHz (the 6-31G(d) basis set) to $A_N = 11.22$ MHz (the 6-311G(d) basis set) or $A_N = 10.88$ MHz (single point calculations at the UB3LYP/6-311++G(3df,2p)//UB3LYP/6-31G(d) level). A more dramatic difference in the ^{14}N hfcc of **1a** is observed for the calculations with Dunning's basis sets: $A_N = 19.67$ MHz for the cc-VDZ and $A_N = 7.95$ MHz for the cc-VTZ basis set. This trend is observed for all considered radicals, as shown in Table 5, and is reflected in the scaling factors *m* listed in Table 6. Hfcc for ^{14}N and ^{1}H generally decrease, while ^{33}S hfcc values increase with the addition of df functions to the 6-31G(d) basis set.

Generally, the UB3LYP/6-31G(d) method appears to give satisfactory results for ^{14}N, ^{1}H, and ^{19}F hfcc, but better correlation factors R^2 are obtained with Dunning's basis sets. The incidental agreement between observed and UB3LYP/6-31G(d) derived hfcc values, reflected in slopes *m* close to unity, is consistent with previous findings for simple organic radicals[40−43] and the results of UB1LYP/6-31G(d) calculations for four heterocyclic radicals.[37]

Calculations of ^{14}N hfcc with geometry optimization at the B3LYP/cc-pVDZ level of theory do not improve the statistics or the linear correlation, based on a comparison of the results for eight data points with analogous sets obtained with either UB3LYP/6-31G(d) calculations or single-point calculations at the UB3LYP/cc-pVDZ//UB3LYP/6-31G(d) level. Similarly, little benefit is offered by geometry optimization and hfcc calculations at the UB3LYP/6-31G(2df) level of theory.

The accuracy of the calculated ^{33}S hfcc is generally much poorer than that observed for the first row elements, and the 6-31G(d) basis set is completely inadequate. The addition of high angular momentum functions partially improves the calculated ^{33}S hfcc, but the closest and satisfactory agreement with the experiment is obtained when the cc-pVDZ basis set is used.

A relatively small mean error (≤0.54 MHz) for the ^{1}H hfcc is observed for single point calculations with the 6-31G(2df) or cc-pVDZ basis sets at the geometry obtained with the 6-31G(d) basis set. Results of calculations done with geometry optimization using the 6-31G(2df) basis set indicate that even smaller mean errors can be obtained, but this correlation is based on only six data points. Inclusion of one p function per hydrogen atom gives an insignificant improvement (≤ 4%) in the STD. All of these analyses exclude the A_H for **1a**, whose reported hfcc value (1.55 MHz)[35] is much smaller than the calculated value, ranging from 4.62 MHz (UB3LYP/cc-pVDZ//UHF/6-31G(d)) to 6.24 MHz (UB3LYP/6-31G(d)). The origin of this unusual discrepancy is not clear.

The mean error for the ^{19}F hfcc is smallest for the UB3LYP/6-31G(d) (−0.33 MHz) and UB3LYP/cc-pVDZ//UHF/6-31G(d) (−0.24 MHz) calculations. However, a meaningful statistical analysis of the calculated ^{19}F hfcc is hindered by the small size of the data set, which contains only four pairs of numbers.

There is only one experimental value for the $^{35/37}$Cl hfcc reported for **4c**[27], and it is consistent with the DFT results. The weight-averaged hfcc for the chlorine natural isotope composition is relatively insensitive to the basis set, and the calculated values fall in the range of −2.0 to −2.5 MHz, which compares to the reported 1.74 MHz for **4c**. A similar value of about −2.3 MHz is calculated for **1c**.

The linear regression analysis for these data sets, shown for selected cases in Figure 3, gives the best fit linear functions collected in Table 6. The intercept was set to 0 to avoid a residual hfcc. The slopes *m* and the correlation factors R^2 are consistent with the results for the alternative error analysis shown in Table 5. All DFT calculations give excellent correlation with the experimental ^{14}N hfcc values with $R^2 \geq 0.98$ and the errors on the calculated slopes in the range of 1.2% (single point at UB3LYP/cc-pVDZ) to 1.7% (UB3LYP/6-31G(2df)). The slopes vary between 0.760 and 1.232 and the value closest to unity is obtained with UB3LYP/6-31G(d) method.

Similar results are obtained for the ^{1}H hfcc with the correlation factors R^2 of about 0.93 and the error on the slopes of about 5% with the noticeable exception for the UB3LYP/6−31(2df) results, for which the R^2 is 0.80 and the slope error is 9.5%. In contrast, the correlation factor R^2 for the ^{33}S hfcc strongly depends on the basis sets used in the calculations. The best correlation ($R^2 = 0.920$) and the smallest error on the slope (1.9%) is obtained for single-point calculations using the cc-pVDZ basis set at the UHF/6-31G(d) geometry. The single-point calculations at the UB3LYP/6-31G(d) geometry also give acceptable results with a slightly larger error on the slope (2.5%).

The fit to a linear function $A_{exp} = m \bullet A_{calc} + b$ shows that the intercept *b* generally is within 2−3 σ for the ^{14}N data set, 1−2

σ for the ^{1}H data set, and $< 1\ \sigma$ for the ^{33}S data set. This further justifies the use of the truncated linear fit for all of the data sets.

Analysis of the distribution of the error in a function of the calculated hfcc suggests that a second-order polynomial may provide a better fit to the data sets. Indeed, fitting the $A_{exp} = m \bullet A_{calc}(A_{calc} + b)$ function to the ^{14}N data gives a significant increase in R^2 (> 0.99) and reduction of χ^2 to about 50% as compared to the linear fit $A_{exp} = m \bullet A_{calc}$. This is not the case for both the ^{1}H and ^{33}S data for which the quadratic functions have significant intercept values of about 1.5 and >6 MHz, respectively, and the improvement of the correlation parameters is only modest.

The hfcc values are sensitive to experimental conditions and a direct comparison between different measurements requires a significant margin of tolerance. Hyperfine coupling values show a weak solvent and temperature dependence, and the range of values exceeds the instrumental error (>±10.03 MHz). A typical nitrogen hfcc shows a positive temperature dependence with an average of 3×10^{-4} mT/K (8×10^{-3} MHz/K), while hydrogen hfcc exhibits smaller negative dependence and the values typically are about -1×10^{-4} mT/K (-3×10^{-3} MHz/K).[29,30,59] These trends are reversed for only one compound (**2d**) in the considered series.[59] Since some of the reported hfcc were obtained at temperatures as low as −90 °C, the hfcc may be different from those at ambient temperature by up to 1 MHz. An additional issue for ^{33}S hfcc is the low natural abundance of the isotope (0.7%) and hence possible lower precision of the measurement for samples that are not isotopically enriched.

The overall reliability and consistency of the experimental data can be estimated at about ±0.5 MHz (±0.02 mT). This value is comparable with an uncertainty of about 1 MHz observed for the correlation between the experimental and best calculated hfcc values for all four nuclei.

The calculations reveal that hfcc values are geometry dependent and differ for each conformer. The difference is minimal for conformers of **1d**, **1e**, and **3e**, moderate (<7%) for **4e** and phenyl substituted compounds **1g** and **4g**, and significant (up to 1 MHz or 40%) for **2d**, especially for the S and N atoms directly affected by the changes in the orientation of the methyl group. As the temperature increases, the molecular geometry is less restricted to that at the minimum of the potential energy surface, and the hfcc becomes a weighted average of the contributions from the ground and thermally populated rotomers in addition to the skeletal thermal vibration effect.[30] This model is consistent with the experimentally observed trends in the hfcc temperature dependence including that for **2d** (vide supra).

The generally excellent performance of the DFT methods in reproducing experimental hfcc allows for critical examination of some cases where either the hfcc or structural assignments are ambiguous. For instance, the DFT calculations consistently indicate that the ^{1}H hfcc in **9i** might be misassigned,[66] as is shown in Figure 4. Simply switching the positions of the hydrogen atoms gives a much better correspondence between the experimental and calculated values.

Experimental data for **7i** allowed for identification of only one ^{1}H hfcc, and its assignment is ambiguous.[71] Using higher resolution techniques and better simulation packages, the complete assignment should be possible based on the predicted values shown in Figure 4.

The calculated hfcc for **12**,[78] the structure initially assigned for **7h**, are substantially larger than the experimental values. The large calculated values are due, in part, to poor N−S overlap ($d_{NS} = 1.780$ Å; cf $d_{NS} = 1.658$ Å in **7h**) and hence large spin

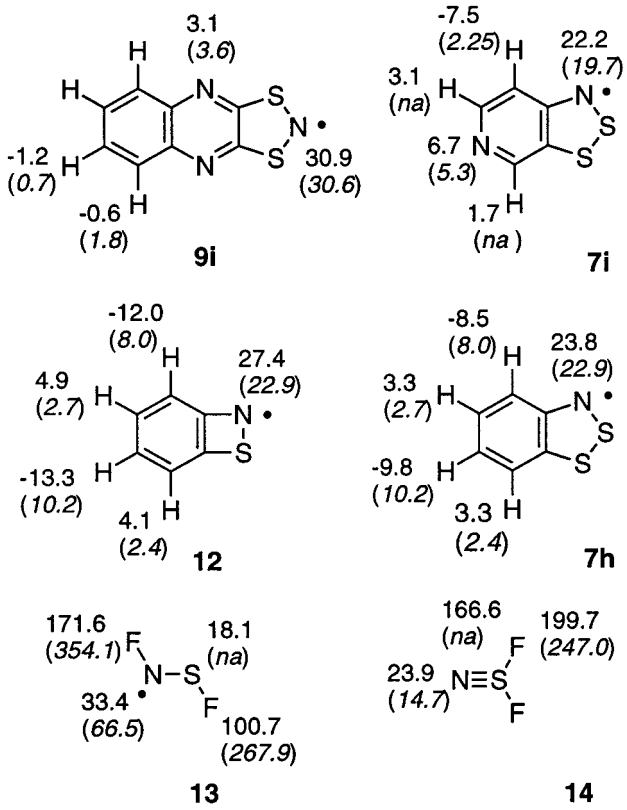

Figure 4. Calculated and reported (in parentheses) hfcc in MHz for selected radicals. The ^{1}H and ^{14}N hfcc were obtained using the UB3LYP/cc-pVDZ//UB3LYP/6-31G(d) method; the ^{19}F hfcc with the UB3LYP/6-31G(d) method, and ^{33}S hfcc values with the UB3LYP/cc-pVDZ//UHF/6-31G(d) method. Each calculated value was scaled using an appropriate factor listed in Table 6.

density on the N atom. The experimental values correspond well to those calculated for **7h** supporting structural reassignment based on substituent effect studies.[71]

The DFT results are in disagreement with the experimental data[79] for the F−N−S−F radical **13**, while the hfcc for its isomer, radical **14**, are reasonably well reproduced by the calculations. The reported ^{14}N and ^{19}F hfcc for **13** are about twice larger than the calculated values, which puts in question the molecular structure assigned to the observed radical species. Radical **14** is pyramidalized, with C_s symmetry and an ^{2}A′ electronic state, and is about 13 kcal/mol more thermodynamically stable that the nonplanar **13**, based on the UB3LYP/6-31G(d) calculations.

Application of the scaling factors developed for the calculated ^{14}N and ^{1}H hfcc was recently demonstrated in the analysis of complex ESR spectra of two new thioaminyl radicals.[23] The scaled UB3LYP results provided the initial guess for numerical simulation. The mean difference between 18 calculated (and scaled) and experimental data points is <0.01 mT, and the estimated standard deviation is 0.02 mT.[23]

Spin Density. The distribution of the total spin density in radicals **1**−**11** (Figure 1) was calculated with the UB3LYP/6-31G* method and results are shown graphically in Figure 5. Calculation with different basis sets gave similar results, indicating only modest sensitivity to the basis set.

Generally, the largest calculated spin density is on the nitrogen atom of the thioaminyl fragment, with the exception of **4c**, in which a significant spin density resides on the sulfur atom and the remaining is almost evenly distributed over the three nitrogen atoms. In systems **2**, **3**, **5**, **6**, **9**, and **10**, the spin density is localized on the −S−N−S− fragment with minor spin distribu-

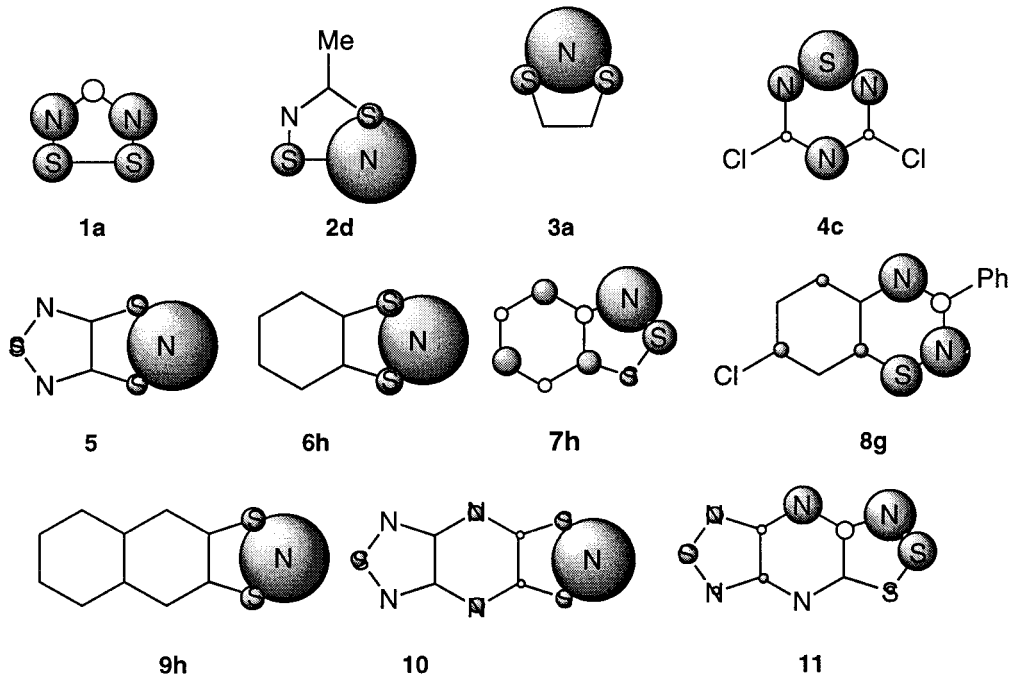

Figure 5. Calculated (UB3LYP/6-31G(d)) total spin density maps for selected radicals **1**−**11**. Circles represent relative total positive (full circles) and negative (open circles) spin densities.

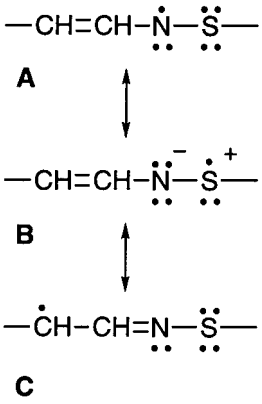

Figure 6. Resonance forms of the vinylthioaminyl fragment.

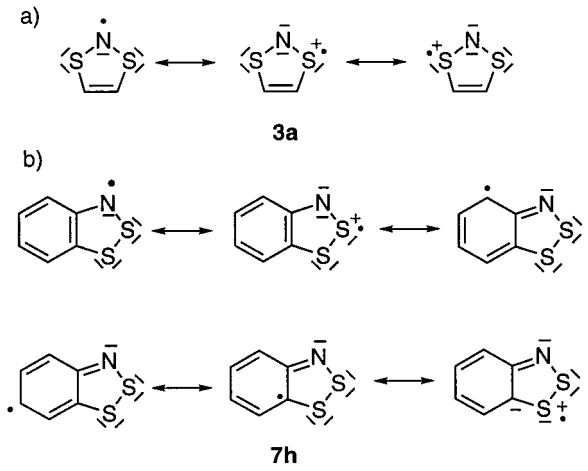

Figure 7. Resonance forms of **3a** (a) and **7h** (b).

tion onto the π framework, presumably through a spin polarization mechanism. In contrast, the remaining systems **1**, **4**, **7**, **8**, and **11** show significant delocalization of the spin density from the nitrogen atom. The substitution sites in **1** and **4** coincide with the nodal planes (negative spin densities), and only **7** and **8** offer the possibility for further spin delocalization onto the substituents.

The calculated distribution of spin density in **1**−**11** is consistent with analysis of the vinylthioaminyl fragment shown in Figure 6. The three resonance structures indicate that the spin density is delocalized from the nitrogen atom (**A**) primarily onto the sulfur atom, giving rise to the polar resonance structure **B**, and the β position (allylic) of the vinyl group (**C**). The α position of the vinyl group has a node. Thus the N-terminated arrays of heteroatoms (e.g., −N−S−S−) allow for significant spin delocalization in the heterocyclic π system, while in the −S−N−S− array, terminated with sulfur atoms, the spin is largely localized on the three-atom fragment.

For instance, in 1,3,2-dithiazolyl (**3a**) virtually all positive spin density is localized on the −S−N−S− array due to two polar resonance structures shown in Figure 7a. A very similar spin distribution is observed in ring-fused derivatives of **3a**, heterocycles **5**, **6h**, **9h**, and **10**, and also **2** (Figure 5). In contrast, a significant spin delocalization is found in **7a**, a benzo-annulated 1,2,3-dithiazolyl derivative containing the −N−S−S− array. In addition to polar resonance forms (**B** in Figure 6), there are also nonpolar allylic-type resonance forms (**C** in Figure 6) allowing for spin delocalization onto the adjacent benzene ring (Figure 7b).

A similar high degree of spin delocalization is observed in **11**, which also contains the −N−S−S− array of heteroatoms. In this case, however, the spin is delocalized primarily along the linear 1,3,5-triazapentadienyl fragment terminated with sulfur atoms. Thiatriazinyl (**4a**) can also be viewed as 1,3,5-triazapentadienyl terminated with a common sulfur atom (Figure 1), which is consistent with the calculated spin density (Figure 5). Likewise, dithiadiazolyl (**1a**) can be considered to be a 1,3-diazaallyl system terminated with sulfur atoms. In a consequence, the positive spin density is delocalized over the nitrogen atoms (allylic resonance form **C**) and sulfur atoms (polar resonance form B in Figure 6), while the carbon atom is in the nodal position and has a negative spin density. In **8g**, one

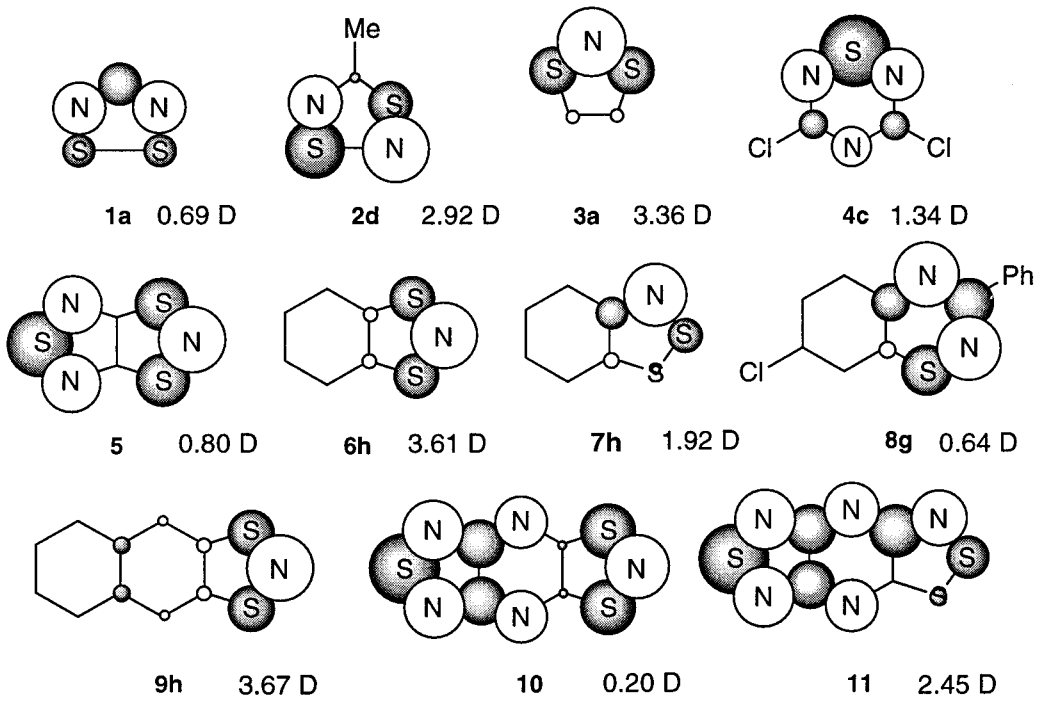

Figure 8. Mulliken total atomic charge density maps (≥ 7%) and dipole moments derived from UB3LYP/6-31G(d) level calculations for selected radicals. Hydrogen atomic charges are included in the charges of adjacent carbon atoms. Circles represent relative total positive (full circles) and negative (open circles) charge densities.

terminus of the diazaallyl system is connected to the adjacent benzene ring, allowing for further spin delocalization (Figure 5).

The calculated spin distributions are consistent with the observed hyperfine coupling constants. Unfortunately, no experimental data for cyclic thioaminyl radicals is available, and the accuracy of the calculated spin densities cannot be verified by direct comparison. The good agreement between theory and experimental data for TCNE radical anion reported in the literature[49] indicates, however, that DFT methods are reliable in the analysis of spin density in radicals.

Charge Distribution and Dipole Moments. The distribution of electron density calculated for radicals **1**−**11** is largely a consequence of the relative atomic electronegativities (S < C < Cl < N) and polar resonance structures analogous to **B** in Figure 6. The electronegative nitrogen atoms display the highest electron density, while the less electronegative sulfur atoms bear the most positive charge as shown in Figure 8. The carbon atoms adjacent to the heteroatoms are polarized appropriately. They are either significantly positively charged, when connected to a nitrogen atom, or bear a small negative charge in the presence of a sulfur atom.

The calculated dipole moments for the radicals are consistent with the electron density distributions and vary from 0.20 D for **10** to about 3.5 D for 1,3,2-dithiazolyls **3a**, **6h**, and **9h**.

Summary and Conclusions

In an effort to develop a theoretical tool for designing new molecular materials, we investigated the dependence of the method (HF and B3LYP) and basis set on molecular parameters (geometry, isotropic hyperfine coupling constants, and spin density) for 23 known heterocyclic radicals containing the thioaminyl fragment. The UHF method reproduces the molecular geometry of two radicals (**1e** and **3e**) significantly better than DFT, but it is inadequate for electronic structure calculations. Excellent or satisfactory correlations for hfcc of all 23 radicals belonging to five general classes (except for A_H of **1a**) and consistent spin densities were found with B3LYP calculations.

Conformational analysis of the heterocyclic derivatives shows that the barriers to internal rotation of the CH_3 and CF_3 groups are generally small, about 1.5 kcal/mol, while that of the Ph group is about 4 times higher. Both methods, the UHF and UB3LYP, generally agree on the conformational ground state for the radicals, with the exception for **1d** and **1e**. In radicals **1g**, **2d**, **4e**, and **4g** the CX_3 and Ph groups generally prefer the eclipsed conformational minima, while in **3e** the CF_3 is pseudo staggered.

The most cost-effective method for computing molecular geometries with acceptable accuracy appears to be the UHF/6-31G(d) (mean error = 0.5 pm and STD = 1.8 pm), while more accurate calculations of the parameters involving the sulfur atom require high angular momentum functions. Thus, for the 6-31G(2df) basis set, the mean error decreases to 0.2 pm, while the STD remains about 1.8 pm (three times the experimental uncertainty).

In the analysis of the hfcc data, the emphasis was placed on the quality of correlation rather than on absolute accuracy of the calculated values, which show a significant basis set sensitivity. Statistical analysis of the results shows that for each nucleus there is a preferred basis set giving maximum consistency of the calculated hfcc and a scaling factor relating the theoretical and experimental values. The best results for ^{14}N (scaling factor = 0.767), ^{1}H (scaling factor = 0.863), and ^{19}F hfcc (scaling factor = 0.806) are obtained using the UB3LYP/cc-pVDZ method at the UB3LYP/6-31G(d) geometry. This method also provides acceptable values for ^{33}S hfcc (scaling factor = 1.252), but best results are obtained using the UHF/6-31G(d) geometry for the UB3LYP/cc-pVDZ single-point calculation (scaling factor = 1.231). The UB3LYP/6-31G(d) is the least expensive method and provides acceptable values for ^{14}N (scaling factor = 0.937), ^{1}H (scaling factor = 0.744), and ^{19}F hfcc (scaling factor = 0.953) hfcc. The estimated accuracy of the these methods is about ±0.2 G, which is close to the

reliability of all experimental data from variety of sources. Conformational mobility has only a small effect on the hfcc values. The application of the resulting scaling factors was demonstrated in critical evaluation of literature data for several radicals.

Analysis of the electronic structures for the radicals shows that the N-terminated array of heteroatoms generally allows for spin delocalization to the adjacent π system, while sulfur atoms cut off the delocalization. Calculations show that in all cases most spin density resides on the −S−N− fragment and is significantly delocalized throughout the π system only in **4**, **7**, **8**, and **11**. Among these, only heterocycles **7** and **8** have positive spin densities at the potential substitution sites and hence are capable of extending further the spin delocalization onto substituents.

Overall, the calculations and established correlations presented here will be helpful in the analysis of experimental data and design of new materials. Undoubtedly, the methods can further be refined using higher levels of theory and more experimental data accumulated over time.

Acknowledgment. This project was supported by NSF (CHE-9528029) and Vanderbilt University. The author thanks Prof. Larry Schaad for enlightening discussions.

Supporting Information Available: Tables containing calculated SCF energies, hfcc, spin densities and thermodynamic parameters. This material is available free of charge via the Internet at http://pubs.acs.org.

References and Notes

(1) Kaszynski, P. *J. Phys. Chem. A* **2001**, *105*, 7626.

(2) Bryan, C. D.; Cordes, A. W.; Goddard, J. D.; Haddon, R. C.; Hicks, R. G.; MacKinnon, C. D.; Mawhinney, R. C.; Oakley, R. T.; Palstra, T. T. M.; Perel, A. S. *J. Am. Chem. Soc.* **1996**, *118*, 330−338.

(3) Bryan, C. D.; Cordes, A. W.; Fleming, R. M.; George, N. A.; Glarum, S. H.; Haddon, R. C.; MacKinnon, C. D.; Oakley, R. T.; Palstra, T. T. M.; Perel, A. S. *J. Am. Chem. Soc.* **1995**, *117*, 6880−6888.

(4) Cordes, A. W.; Haddon, R. C.; Hicks, R. G.; Kennepohl, D. K.; Oakley, R. T.; Schneemeyer, L. F.; Waszczak, J. V. *Inorg. Chem.* **1993**, *32*, 1554−1558.

(5) Cordes, A. W.; Haddon, R. C.; Oakley, R. T.; Schneemeyer, L. F.; Waszczak, J. V.; Young, K. M.; Zimmerman, N. M. *J. Am. Chem. Soc.* **1991**, *113*, 582−588.

(6) Barclay, T. M.; Cordes, A. W.; Haddon, R. C.; Itkis, M. E.; Oakley, R. T.; Reed, R. W.; Zhang, H. *J. Am. Chem. Soc.* **1999**, *121*, 969−976.

(7) Cordes, A. W.; Haddon, R. C.; Hicks, R. G.; Oakley, R. T.; Vajda, K. E. *Can. J. Chem.* **1998**, *76*, 307−312.

(8) Andrews, M. P.; Cordes, A. W.; Douglass, D. C.; Fleming, R. M.; Glarum, S. H.; Haddon, R. C.; Marsh, P.; Oakley, R. T.; Palstra, T. T. M.; Schneemeyer, L. F.; Trucks, G. W.; Tycko, R.; Waszczak, J. V.; Young, K. M.; Zimmerman, N. M. *J. Am. Chem. Soc.* **1991**, *113*, 3559−3568.

(9) Barclay, T. M.; Cordes, A. W.; George, N. A.; Haddon, R. C.; Oakley, R. T.; Palstra, T. T. M.; Patenaude, G. W.; Reed, R. W.; Richardson, J. F.; Zhang, H. *Chem. Commun.* **1997**, 873−874.

(10) Langley, P. J.; Rawson, J. M.; Smith, J. N. B.; Schuler, M.; Bachmann, R.; Schweiger, A.; Palacio, F.; Antorrena, G.; Gescheidt, G.; Quintel, A.; Rechsteiner, P.; Hulliger, J. *J. Mater. Chem.* **1999**, *9*, 1431−1434.

(11) Antorrena, G.; Davies, J. E.; Hartley, M.; Palacio, F.; Rawson, J. M.; Smith, J. N. B.; Steiner, A. *Chem. Commun.* **1999**, 1393−1394.

(12) Barclay, T. M.; Cordes, A. W.; George, N. A.; Haddon, R. C.; Itkis, M. E.; Oakley, R. T. *Chem. Commun.* **1999**, 2269−2270.

(13) McManus, G. D.; Rawson, J. M.; Feeder, N.; Palacio, F.; Oliete, P. *J. Mater. Chem.* **2000**, *10*, 2001−2003.

(14) Oakley, R. T. *Prog. Inorg. Chem.* **1988**, *36*, 299−391.

(15) Rawson, J. M.; Banister, A. J.; Lavender, I. *Adv. Heterocyc. Chem.* **1995**, *62*, 137−247.

(16) Rawson, J. M.; McManus, G. D. *Coord. Chem. Rev.* **1999**, *189*, 135−168.

(17) Boeré, R. T.; Roemmele, T. L. *Coord. Chem. Rev.* **2000**, *210*, 369−445.

(18) Awere, E. G.; Burford, N.; Mailer, C.; Passmore, J.; Schriver, M. J.; White, P. S.; Banister, A. J.; Oberhammer, H.; Sutcliffe, L. H. *J. Chem. Soc., Chem. Commun.* **1987**, 66−69.

(19) Brooks, W. V. F.; Burford, N.; Passmore, J.; Schriver, M. J.; Sutcliffe, L. H. *J. Chem. Soc., Chem. Commun.* **1987**, 69−71.

(20) Patel, M. K.; Huang, J.; Kaszynski, P. *Mol. Cryst. Liq. Cryst.* **1995**, *272*, 87−97.

(21) Kaszynski, P. In *Magnetic Properties of Organic Materials*; Lahti, P. M., Ed.; Dekker: New York, 1999; pp 305−324.

(22) Farrar, J. M.; Patel, M. K.; Kaszynski, P.; Young, V. G., Jr. *J. Org. Chem.* **2000**, *65*, 931−940.

(23) Benin, V.; Kaszynski, P. *J. Org. Chem.* **2000**, *65*, 8086−8088.

(24) Hayes, P. J.; Oakley, R. T.; Cordes, A. W.; Pennington, W. T. *J. Am. Chem. Soc.* **1985**, *107*, 1346−1351.

(25) Boeré, R. T.; Cordes, A. W.; Hayes, P. J.; Oakley, R. T.; Reed, R. W.; Pennington, W. T. *Inorg. Chem.* **1986**, *25*, 2445−2450.

(26) Boeré, R. T.; Moock, K. H.; Parvez, M. *Z. Anorg. Allg. Chem.* **1994**, *620*, 1589−1598.

(27) Boeré, R. T.; Oakley, R. T.; Reed, R. W.; Westwood, N. P. C. *J. Am. Chem. Soc.* **1989**, *111*, 1180−1185.

(28) Höfs, H.-U.; Bats, J. W.; Gleiter, R.; Hartmann, G.; Mews, R.; Eckert-Maksic, M.; Oberhammer, H.; Sheldrick, G. M. *Chem. Ber.* **1985**, *118*, 3781−3804.

(29) MacLean, G. K.; Passmore, J.; Rao, M. N. S.; Schriver, M. J.; White, P. S.; Bethell, D.; Pilkington, R. S.; Sutcliffe, L. H. *J. Chem. Soc., Dalton Trans.* **1985**, 1405−1416.

(30) Fairhurst, S. A.; Pilkington, R. S.; Sutcliffe, L. H. *J. Chem Soc., Faraday Trans. 1*, **1983**, *79*, 925−940.

(31) Barclay, T. M.; Cordes, A. W.; Goddard, J. D.; Mawhinney, R. C.; Oakley, R. T.; Preuss, K. E.; Reed, R. W. *J. Am. Chem. Soc.* **1997**, *119*, 12136−12141.

(32) Barclay, T. M.; Cordes, A. W.; de Laat, R. H.; Goddard, J. D.; Haddon, R. C.; Jeter, D. Y.; Mawhinney, R. C.; Oakley, R. T.; Palstra, T. T. M.; Patenaude, G. W.; Reed, R. W.; Westwood, N. P. C. *J. Am. Chem. Soc.* **1997**, *119*, 2633−2641.

(33) Cordes, A. W.; Goddard, J. D.; Oakley, R. T.; Westwood, N. P. C. *J. Am. Chem. Soc.* **1989**, *111*, 6147−6154.

(34) Campbell, J.; Klapstein, D.; Bernath, P. F.; Davis, W. M.; Oakley, R. T.; Goddard, J. D. *Inorg. Chem.* **1996**, *35*, 4264−4266.

(35) Cordes, A. W.; Bryan, C. D.; Davis, W. M.; de Laat, R. H.; Glarum, S. H.; Goddard, J. D.; Haddon, R. C.; Hicks, R. G.; Kennepohl, D. K.; Oakley, R. T.; Scott, S. R.; Westwood, N. P. C. *J. Am. Chem. Soc.* **1993**, *115*, 7232−7239.

(36) Awere, E. G.; Burford, N.; Haddon, R. C.; Parson, S.; Passmore, J.; Waszczak, J. V.; White, P. S. *Inorg. Chem.* **1990**, *29*, 4821−4830.

(37) Mattar, S. M.; Stephens, A. D. *Chem. Phys. Lett.* **2000**, *327*, 409−419.

(38) *Recent Advances in Density Functional Methods*; Chong, D. P., Ed.; World Scientific: Singapore, 1995.

(39) Becke, A. D. *Phys. Rev. A* **1988**, *38*, 3098−3100.

(40) Jaszewski, A. R.; Jezierska, J.; Jezierski, A. *Chem. Phys. Lett.* **2000**, *319*, 611−617.

(41) Adamo, C.; Barone, V.; Fortunelli, A. *J. Phys. Chem.* **1995**, *99*, 384−393.

(42) Qin, Y.; Wheeler, R. A. *J. Chem. Phys.* **1995**, *102*, 1689−1698.

(43) Barone, V. *Theor. Chim. Acta* **1995**, *91*, 113−128.

(44) Walden, S. E.; Wheeler, R. A. *J. Chem. Soc., Perkin Trans. 2*, **1996**, 2663−2672.

(45) Gauld, J. W.; Eriksson, L. A.; Radom, L. *J. Phys. Chem.* **1997**, *101*, 1352−1359.

(46) Becke, A. D. *J. Chem. Phys.* **1993**, *98*, 5648−5652.

(47) Cohen, M. J.; Chong, D. P. *Chem. Phys. Lett.* **1995**, *234*, 405−412.

(48) Jaszewski, A. R.; Jezierska, J.; Krowicka, M.; Kalecinska, E. *Appl. Magn. Res.* **2000**, *18*, 85−100.

(49) Zheludev, A.; Grand, A.; Ressouche, E.; Schweizer, J.; Morin, B. G.; Epstein, A. J.; Dixon, D. A.; Miller, J. S. *J. Am. Chem. Soc.* **1994**, *116*, 7243−7243.

(50) Jursic, B. S. *THEOCHEM* **1998**, *432*, 211−217.

(51) Gaussian 94, Revision E.1, Frisch, M. J.; Trucks, G. W.; Schlegel, H. B.; Gill, P. M.; Johnson, B. G.; Robb, M. A.; Cheeseman, J. R.; Keith, T.; Petersson, G. A.; Montgomery, J. A.; Raghavachari, K.; Al-Laham, M. A.; Zakrzewski, V. G.; Ortiz, J. V.; Foresman, J. B.; Cioslowski, J.; Stefanov, B. B.; Nanayakkara, A.; Challacombe, M.; Peng, C. Y.; Ayala, P. Y.; Chen, W.; Wong, M. W.; Andres, J. L.; Replogle, E. S.; Gomperts, R.; Martin, R. L.; Fox, D. J.; Binkley, J. S.; Defrees, D. J.; Baker, J.; Stewart, J. P.; Head-Gordon, M.; Gonzalez, C.; Pople, J. A.; Gaussian, Inc.: Pittsburgh, PA, 1995.

(52) Frisch, M. J.; Pople, J. A.; Binkley, J. S. *J. Chem. Phys.* **1984**, *80*, 3265−3269.

(53) Woon, D. E.; Dunning, T. H. J. *J. Chem. Phys.* **1993**, *98*, 1358−1371.

(54) Lee, C.; Yang, W.; Parr, R. G. *Phys. Rev. B*, **1988**, *37*, 785−789.

(55) Scott, A. P.; Radom, L. *J. Phys. Chem.* **1996**, *100*, 16502−16513.
(56) Foresman, J. B.; Frisch, A. *Exploring Chemistry with Electronic Structure Methods*; Gaussian, Inc.: Pittsburgh, PA, 1996.
(57) Results of hfcc calculations using Gaussian 98 are also listed in MHz and Gauss units.
(58) Preston, K. F.; Sutcliffe, L. H. *Magn. Reson. Chem.* **1990**, *28*, 189−204.
(59) Fairhurst, S. A.; Johnson, K. M.; Sutcliffe, L. H.; Preston, K. F.; Banister, A. J.; Hauptman, Z. V.; Passmore, J. *J. Chem. Soc., Dalton Trans.* **1986**, 1465−1472.
(60) Fairhurst, S. A.; Sutcliffe, L. H.; Preston, K. F.; Banister, A. J.; Partington, A. S.; Rawson, J. M.; Passmore, J.; Schriver, M. J. *Magn. Reson. Chem.* **1993**, *31*, 1027−1030.
(61) Markovski, L. N.; Polumbrik, O. M.; Talanov, V. S.; Shermolovich, Y. G. *Tetrahedron Lett.* **1982**, *23*, 761−762.
(62) Harrison, S. R.; Pilkington, R. S.; Sutcliffe, L. H. *J. Chem. Soc., Faraday Trans. 1*, **1984**, *80*, 669−689.
(63) Chung, Y.-L.; Sandall, J. P. B.; Sutcliffe, L. H.; Joly, H.; Preston, K. F.; Johann, R.; Wolmershäuser, G. *Magn. Reson. Chem.* **1991**, *29*, 625−630.
(64) Barclay, T. M.; Cordes, A. W.; George, N. A.; Haddon, R. C.; Itkis, M. E.; Mashuta, M. S.; Oakley, R. T.; Patenaude, G. W.; Reed, R. W.; Richardson, J. F.; Zhang, H. *J. Am. Chem. Soc.* **1998**, *120*, 352−360.
(65) Chung, Y.-L.; Fairhurst, S. A.; Gillies, D. G.; Preston, K. F.; Sutcliffe, L. H. *Magn. Reson. Chem.* **1992**, *30*, 666−672.
(66) Chung, Y.-L.; Fairhurst, S. A.; Gillies, D. G.; Kraft, G.; Krebber, A. M. L.; Preston, K. F.; Sutcliffe, L. H.; Wolmershäuser, G. *Magn. Reson. Chem.* **1992**, *30*, 774−778.
(67) Wolmershäuser, G.; Kraft, G. *Chem. Ber.* **1990**, *123*, 881−885.
(68) Dormann, E.; Nowak, M. J.; Williams, K. A.; Angus, R. O. J.; Wudl, F. *J. Am. Chem. Soc.* **1987**, *109*, 2594−2599.
(69) Preston, K. F.; Sandall, J. P. B.; Sutcliffe, L. H. *Magn. Reson. Chem.* **1988**, *26*, 755−759.
(70) Mayer, R.; Domschke, G.; Bleisch, S.; Bartl, A.; Staško, A. *Z. Chem.* **1981**, *21*, 264−265.
(71) Mayer, R.; Domschke, G.; Bleisch, S.; Fabian, J.; Bartl, A.; Staško, A. *Collect. Czech. Chem. Commun.* **1984**, *49*, 684−703.
(72) Markovskii, L. N.; Talanov, V. S.; Polumbrik, O. M.; Shermolovich, Y. G. *J. Org. Chem. USSR* **1981**, *17*, 2338−2339.
(73) Mattar, S. M.; Stephens, A. D. *J. Phys. Chem. A* **2000**, *104*, 3718−3732.
(74) Vegas, A.; Pérez-Salazar, A.; Banister, A. J.; Hey, R. G. *J. Chem. Soc., Dalton Trans.* **1980**, 1812−1815.
(75) Scholz, U.; Roesky, H. W.; Schimkowiak, J.; Noltemeyer, M. *Chem. Ber.* **1989**, *122*, 1067−1070.
(76) Hazell, A.; Hazell, R. G. *Acta Crystallogr., Sect. C* **1988**, *C44*, 1807−1810.
(77) McConnell, H. M. *J. Chem. Phys.* **1956**, *24*, 764−766.
(78) Mayer, R.; Bleisch, S.; Domschke, G.; Tkáč, A.; Staško, A.; Bartl, A. *Org. Magn. Res.* **1979**, *12*, 532−534.
(79) Boate, A. R.; Preston, K. F. *Inorg. Chem.* **1978**, *17*, 1669−1670.